ACS APPLIED MATERIALS & INTERFACES

www.acsami.org

Research Article

Effect of Core Oligomer Length on the Phase Behavior and Assembly of π-Conjugated Peptides

Edward R. Jira, Kirill Shmilovich, Tejaswini S. Kale, Andrew Ferguson, John D. Tovar, and Charles M. Schroeder*

Cite This: *ACS Appl. Mater. Interfaces* 2020, 12, 20722–20732

Read Online

ACCESS | Metrics & More | Article Recommendations | Supporting Information

ABSTRACT: Biohybrid molecules are a versatile class of materials for controlling the assembly behavior and functional properties of electronically active organics. In this work, we study the effect of the size of the π-conjugated core on the assembly and phase behavior for a series of π-conjugated peptides consisting of oligothiophene cores of defined lengths flanked by sequence-defined peptides (OT*X*, where *X* = 4, 5, 6 is the number of thiophene core units). Interestingly, we find that π-conjugated peptides with relatively short OT4 cores assemble into ordered, high aspect ratio, one-dimensional (1D) structures, whereas π-conjugated peptides with longer OT5 and OT6 cores assemble into disordered structures or lower aspect ratio 1D structures depending on assembly conditions. Phase diagrams for assembled materials are experimentally determined as a function of ionic strength, pH, temperature, and peptide concentration, revealing the impact of molecular sequence and π-conjugated core length on assembled morphologies. Molecular dynamics (MD) simulations are further used to probe the origins of microscale differences in assembly that arise from subtle changes in molecular identity. Broadly, our work elucidates the mechanisms governing the assembly of π-conjugated peptides, which will aid in efficient materials processing for soft electronic applications. Overall, these results highlight the complex phase behavior of biohybrid materials, including the impact of molecular sequence on assembly behavior and morphology.

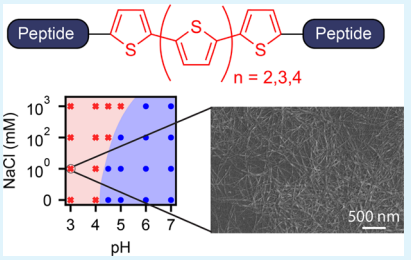

KEYWORDS: *π-conjugated peptides, self-assembly, phase diagrams, sequence controlled, biohybrid electronics*

INTRODUCTION

Electronically active organic materials offer strong promise for applications in next-generation soft electronic devices. In recent years, transistors based on organic semiconductors have been used to develop electronic devices with applications including flexible electronic displays,[1] wearable electronics,[2] and pressure sensors for artificial skins.[3] Owing to the immense diversity and tunability afforded by semiconducting π-conjugated systems, research in this area has yielded organic devices with performance parameters comparable to inorganic devices.[4] Despite recent progress, challenges remain in fabricating consistently reliable devices because of the strong dependence of charge transport on molecular packing[5] and the impact of grain boundaries and defects[6] on device performance.[7,8]

Self-assembling systems offer a potential strategy for controlling intermolecular packing to guide assembly into defined supramolecular structures with desirable charge transport properties. To this end, prior work has focused on cofacial packing of conjugated ring systems that were shown to be optimal for intermolecular charge transport because of significant orbital overlap between neighboring molecules.[9] Self-assembled gels and nanowires have shown early promise for incorporation into organic field-effect transistors[10−12] and organic light-emitting diodes.[13] However, the vast chemical space for organic molecules, combined with challenges in synthesis and the need to simultaneously optimize conductivity and assembled structures, leads to formidable challenges in the design of self-assembled electronic materials.

Biohybrid molecules are promising candidates for controlling the assembly properties of functional materials. In particular, biohybrid molecules benefit from the structural diversity of synthetic molecules, combined with facile sequence control and well-known assembly properties of biomolecules such as peptides and nucleotides.[14] Hybrid molecules consisting of a hydrophobic synthetic moiety covalently linked to a hydrophilic self-assembling peptide structure have been widely studied and shown to assemble into a variety of structures including sheets,[15] tapes,[16] spheres,[17] and fibers.[18,19] Moreover, it has been demonstrated that seemingly minor alterations in peptide sequence at specific locations can lead to drastic differences in assembled morphology.[20−24] Despite recent work, however, we generally lack a complete under-

Received: February 3, 2020
Accepted: April 14, 2020
Published: April 14, 2020

https://dx.doi.org/10.1021/acsami.0c02095
ACS Appl. Mater. Interfaces 2020, 12, 20722−20732

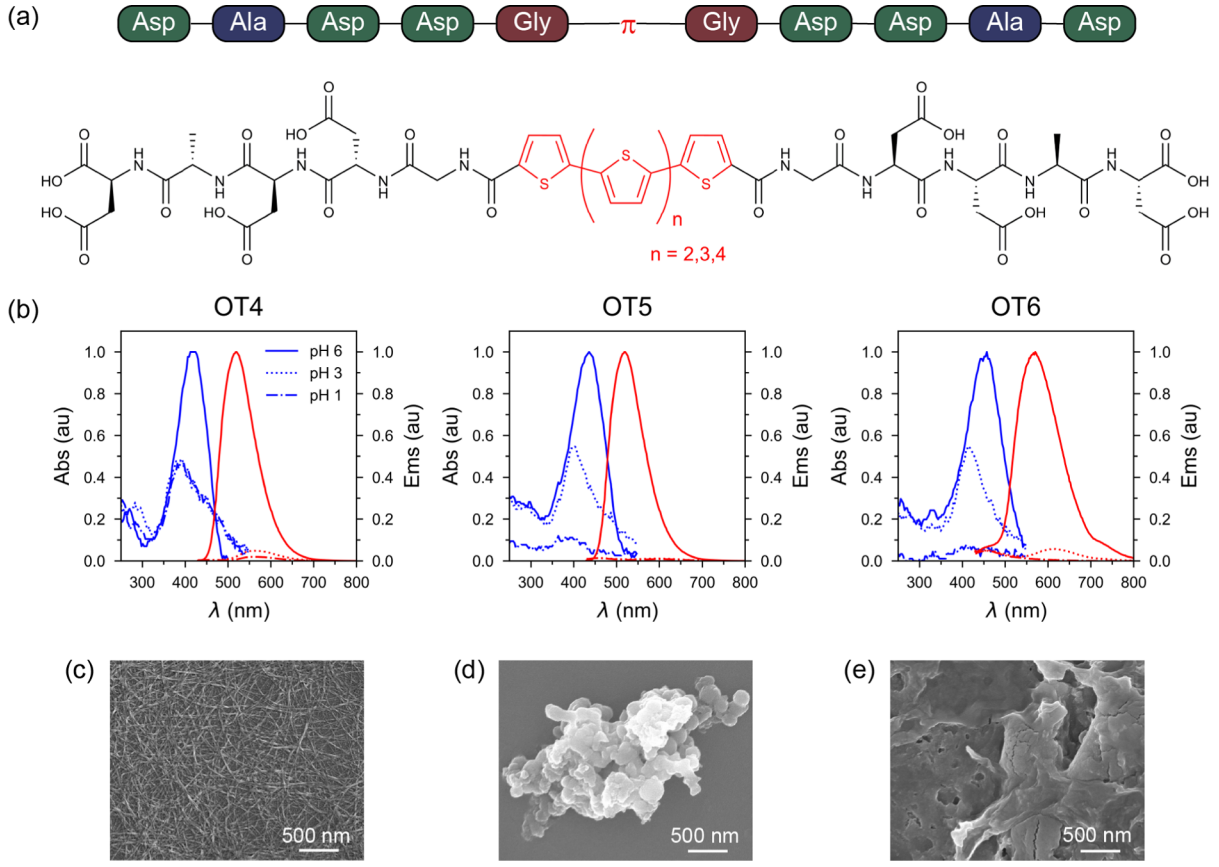

Figure 1. Structural and spectral properties of acid-triggered self-assembled aggregates of OT*X* peptides. (a) Schematic and chemical structure of OT*X* peptides, with the conjugated core shown in red, flanked by symmetric aspartic acid-rich peptide sequences. (b) UV−vis absorbance (blue lines) and fluorescence emission spectra (red lines) of OT*X* peptides at varying pH showing quenching of absorbance and emission and blue-shifted absorbance with decreasing pH. (c) SEM micrograph of OT4 assembled at pH 1 showing a high aspect ratio fiber network. (d,e) SEM micrographs of OT5 and OT6, respectively, assembled at pH 1 showing disordered aggregates upon assembly.

standing of the effect of molecular sequence on the structure−function properties of these materials.

Recently, a class of biohybrid molecules was realized, which included π-conjugated moieties in the central portions (or cores) of molecular structures, symmetrically flanked by sequence-defined peptides on both termini. In this way, water-soluble semiconducting π-conjugated peptides have shown immense promise for soft organic electronics.[25] These molecules are typically designed to incorporate a number of carboxylic acid-containing amino acids into the flanking peptide sequences, thereby preventing spontaneous assembly via electrostatic repulsions when deprotonated under neutral or basic pH conditions. Using this approach, self-assembly can be triggered by transitioning to acidic environments in aqueous solution, thereby relieving electrostatic repulsions between molecules and enabling assembly. Self-assembly is guided by hydrophobicity and π-stacking interactions in adjacent π-conjugated cores, together with hydrogen bonding among the flanking peptide sequences, thereby resulting in ordered one-dimensional (1D) assembled nanowires by simple addition of acid to an aqueous solution[26−28] or by increasing the concentration of π-conjugated peptides for specific sequences.[29]

In 1D assembled structures, π-conjugated cores are locked into a stacked, cofacial arrangement that has been shown to facilitate charge transport for next-generation organic electronic applications. Specifically, printed thin films of these 1D structures can be incorporated as the semiconductor layer in organic electronics where they display high charge carrier mobilities because of their ordered structures.[30] However, preparation of these devices presents additional challenges compared to traditional organic thin-film semiconductors, especially in terms of reliability and repeatability. In order to yield high-performance devices consisting of ordered structures, one must be able to predictably control assembly during processing with consideration given to temperature, conjugated core identity and sequence, and related processing parameters that directly affect assembly. Furthermore, the aqueous solubility of these materials makes them promising candidates as biologically active electronics, which have garnered significant interest for applications in tissue engineering[31] and biologically compatible sensors.[32] However, practical implementation of these devices in a biological setting necessitates a clear understanding of their assembly behavior and morphologies over a wide range of biologically relevant conditions including pH and ionic strength. Overall, π-conjugated peptides are a promising class of biohybrid materials for controlling assembled structures and charge transport properties; however, it is generally known that assembly is sensitive to peptide sequence, π-core chemistry, and a wide range of environmental factors including ionic strength, peptide concentration, temperature, and choice of solvent. From this view, there is a clear need to understand the effect of molecular π-core identity, peptide sequence, and

https://dx.doi.org/10.1021/acsami.0c02095
ACS Appl. Mater. Interfaces 2020, 12, 20722−20732

environmental conditions on the assembled morphologies and phase behavior of π-conjugated peptides.

In this work, we study the phase behavior and assembly properties of π-conjugated peptides containing oligothiophene cores of defined length (OT*X*, where *X* is the number of thiophene units). In particular, we focus on molecules containing oligothiophene cores with four, five, or six units (OT4, OT5, OT6) flanked by symmetric peptides with defined sequence Asp-Ala-Asp-Asp-Gly (DADDG). For these molecules, the N- to C-terminus directionality of the peptide flanking sequences progresses away from the π-core such that each molecule possesses two C termini. We explore the effect of π-conjugated core length on the assembly properties and phase behavior of a series of biohybrid peptides with precisely defined sequences. We begin by using acid-triggered assembly in aqueous solution to characterize the morphologies and optical properties of assembled structures using electron microscopy and UV−vis spectroscopy. Molecular dynamics (MD) simulations are used to understand the molecular origin of microscale differences in assembly that arise from subtle changes in sequence. Moreover, we determine phase diagrams for π-conjugated peptides by driving assembly by addition of excess salt, thereby screening electrostatic repulsions between peptides and triggering assembly. Phase diagrams are experimentally determined by systematically varying pH, ionic strength, and peptide concentration for π-conjugated peptides OT4, OT5, and OT6. Interestingly, we further show that temperature can be used as an additional trigger of assembly, enabling the systematic determination of phase diagrams in temperature−concentration space. Taken together, these results demonstrate the versatility in assembly conditions for these materials, as well as the importance of specifically tuning environmental conditions to yield desired structures and morphologies.

EXPERIMENTAL METHODS

Materials. Sequence-defined symmetric π-conjugated peptides (peptide-π-peptide) were prepared using solid-phase peptide synthesis, as previously reported (Figures S1-S6).[29,33] π-Conjugated cores containing thiophene 4-, 5-, or 6-mers are flanked by symmetric peptides with an amino acid sequence Asp-Ala-Asp-Asp-Gly with directionality such that each molecule possesses two C termini (Figure 1a). The overall sequence for these molecules is DADDG-OT*X*-GDDAD (*X* = 4, 5, 6; hereafter abbreviated as OT*X* for brevity).

Structural and Optical Characterization. Assembled structures of π-conjugated peptides were characterized using a Hitachi S4800 high-resolution scanning electron microscope. Here, prepared peptide samples are drop-cast onto clean Si wafers and imaged via scanning electron microscopy (SEM) upon drying. UV−visible absorbance spectra were recorded using a Thermo Scientific NanoDrop 1000 spectrophotometer. Transmission electron microscopy (TEM) was performed on a Philips EM 420 transmission electron microscope equipped with an SIS Megaview III CCD digital camera at an accelerating voltage of 100 kV. The samples were prepared by pipetting a drop of 1 mg/mL solution of assembled peptide in water onto 200 mesh copper grids coated with a Formvar film (electron microscopy sciences) and adsorbed for 5 min at room temperature. The grid was washed with deionized (DI) water, and the excess solution was wicked off by touching the side of the grid to a filter paper. The sample was then stained with a 2% uranyl acetate solution and washed with DI water, and excess moisture was wicked off. The grid was allowed to dry in air before imaging. Fluorescence emission spectra were recorded using a Tecan Infinity M200 Pro plate reader at an excitation wavelength of 360 nm.

Dynamic Light Scattering Measurements. Particle size of unassembled and assembled OT6 molecules was characterized using dynamic light scattering (DLS) on a Malvern Zetasizer Nano ZS particle size analyzer. Here, peptides were diluted to a concentration of 0.1 mg/mL and filtered through 200 nm syringe filters. Filtered citrate buffer was then added to a final buffer concentration of 0.1 M and desired pH. DLS measurements were performed on samples in backscatter detection mode.

MD Simulations. The GROMACS 2018.4 simulation suite was used to perform all-atom MD simulations of single and multimolecule OT*X* systems solvated in water.[34] Topologies and initial configurations of single OT*X* molecules were generated using the Automated Topology Builder (ATB) server[35] and modeled with the GROMOS 54a7 force field.[36] Water was modeled using the simple point charge force field.[37] The amino acid side chains were parameterized in the low-pH state such that the Asp side chains and two C-termini are fully protonated, and each OT*X* molecule is charge neutral. Single molecule runs centered each OT*X* molecule in a cubic simulation box with 1.5 nm spacing between the molecule and box edges. Multimolecule simulations randomly placed 60 OT*X* molecules in a 10 × 10 × 10 nm^3 cubic simulation box employing three-dimensional (3D) periodic boundary conditions and corresponding to a concentration of 0.1 mM. Simulations were performed in the *NPT* ensemble at a temperature of 300 K and a pressure of 1 bar using the velocity-rescaling thermostat[38] and Parrinello−Rahman barostat.[39] Initial atom velocities were drawn from a Maxwell−Boltzmann distribution at 300 K. Steepest descent energy minimization was used to correct for high-energy overlaps removing forces larger than 1000 kJ/mol nm, followed by 100 ps of *NVT* equilibration and 100 ps of *NPT* equilibration to ensure that the temperature, pressure, and energy had reached steady values. The leap-frog algorithm[40] with a 2 fs time step was used to numerically integrate forward the equations of motion. Coulombic interactions were treated by particle mesh Ewald[41] employing a real-space cutoff of 1.0 nm and a 0.16 nm Fourier grid spacing that was subsequently optimized during runtime. Covalent bonds involving hydrogens were held fixed during simulations using the LINCS algorithm,[42] and Lennard-Jones interactions were smoothly shifted at 1.0 nm to zero. Following equilibration, *NPT* production runs at 300 K and 1 bar for single molecule simulations were carried out for 30 ns while those for multimolecule systems were carried out for 100 ns.

Determination of pH−Salt Phase Diagrams. OT*X* peptides were dissolved in distilled, DI water (Millipore, conductivity 18 MΩ cm). Aqueous solutions (50 μL) of π-conjugated peptide (0.05 mg/mL) were prepared in 10 mM citrate buffer of specified pH and specified amounts of salt (NaCl or $MgCl_2$). Upon addition of salt, phase change occurred nearly instantaneously. After incubation for several minutes, peptide solutions were centrifuged in a Sorvall Legend RT+ centrifuge (4 h, 3000*g*, 20 °C) to resolve separated phases. After centrifugation, the solution was imaged under UV light to identify the presence of a second phase, followed by determination of absorbance and fluorescence emission spectra of the aqueous phase using a NanoDrop 1000 and Tecan M200 Pro, respectively.

Determination of Temperature−Concentration Phase Diagrams. OT4 peptides were dissolved in distilled, DI water (Millipore, conductivity 18 MΩ cm). Aqueous solutions (50 μL) of π-conjugated peptide (0.05 mg/mL) were prepared in 10 mM citrate buffer (pH 4.5). Aqueous peptide solutions were equilibrated at constant, target temperature for 120 h in a Bio-Rad T100 thermal cycler. After equilibration, the samples were removed and centrifuged in a Sorvall Legend RT+ centrifuge (4 h, 3000*g*, 20 °C) to resolve separated phases. The supernatant aqueous phase was pipetted off and absorbance was measured using a Nanodrop 1000, thereby enabling determination of the π-conjugated peptide concentration of the aqueous phase using the Beer−Lambert law ($A = \epsilon cl$), where A is the absorbance, l is the path length specified by the instrument, and ϵ is the molar extinction coefficient taken to be that of quaterthiophene, as previously reported.[43] In this way, the concentration of π-conjugated peptide in the peptide-rich phase was determined via mass

https://dx.doi.org/10.1021/acsami.0c02095
ACS Appl. Mater. Interfaces 2020, 12, 20722−20732

balance based on the peptide concentration and volume of the initial solutions.

RESULTS

Acid-Triggered Assembly of OT*X* Peptides. We began by using acid-triggered assembly to characterize the self-assembled morphologies and photophysical properties of OT4, OT5, and OT6 (Figure 1). Prior work has shown that π-conjugated peptides with the general symmetric structure peptide-π-peptide assemble into ordered 1D structures that form networks of randomly aligned fibers.[26] Moreover, these assembled structures are often accompanied by distinct spectral signatures such as a quenched, blue-shifted absorbance, indicative of H-type aggregation with coplanar excitonic coupling and π-stacking between molecules as well as quenched, red-shifted emission, likely caused by conformational restriction into a planar form of molecules in assembly.[26,44−46] However, the effect of changing π-core length on the assembly and photophysical properties has not been fully elucidated in these types of peptide-π molecules.

Assembly was triggered by the direct addition of acid (concentrated hydrochloric acid, HCl) to aqueous peptide solutions (0.05 mg/mL OT*X*) to pH ≈ 1. Upon addition of acid, OT4, OT5, and OT6 exhibited quenched, blue-shifted absorbance spectra and quenched fluorescence emission spectra, indicative of assembly (Figures 1b and S7). Blue-shifted, quenched absorbance is generally consistent with H-type aggregate behavior,[47] suggesting an ordered cofacial packing of molecules into 1D supramolecular wires. Interestingly, the fluorescence emission spectra revealed unexpected behavior for peptides with different length π-conjugated cores. In particular, OT4 was found to exhibit a red-shifted emission spectrum that is generally consistent with prior studies on π-conjugated peptides with quaterthiophene cores but different peptide sequences.[26,29,48] However, OT5 and OT6 exhibit both blue-shifted and red-shifted fluorescence emission peaks, indicating the possibility of a drastically different hierarchical assembled structure compared to ordered 1D assembled fibers reported in prior work.

We further characterized assembled morphologies using SEM. After triggering assembly with acid, the peptide solution was pipetted onto a silicon substrate and allowed to dry, followed by SEM imaging. Assembled OT4 shows a dense fiber structure, consistent with prior studies on the assembly of π-conjugated peptides with different peptide sequences.[26,45,46] Assembled fibers show high aspect ratios with nanometer widths and lengths exceeding 1 μm (Figure 1c). Unexpectedly, the SEM images of OT5 and OT6, under the same acid-triggered assembly conditions, were dominated by several large, irregularly shaped aggregate structures with dimensions on the order of several hundred nanometers or larger (Figure 1d,e). These results are consistent with DLS measurements on OT6 peptides (Figure S8) as well as with TEM images of these samples, which show high aspect ratio fibers for OT4 (Figure S9) and less ordered, low aspect ratio structures for OT5 and OT5 (Figures S10 and S11). Interestingly, prior work has observed evidence of small fibers for assembled OT5 and OT6 peptides assembled under different conditions. However, these structures occur on smaller length scales (10−20 nm) compared to the microscale, long-range assemblies observed for OT4.[48] This suggests that OT5 and OT6 might be capable of forming 1D structures under certain assembly conditions but generally show lower propensity for order than their shorter π-core counterparts.

Given these results, we hypothesized that OT*X* peptides with longer π-conjugated cores might be preferentially exhibiting intramolecular rather than intermolecular interactions under the present conditions in order to minimize π-core repulsion in the aggregates. Here, longer cores may adopt intramolecular hairpin-like folded structures, wherein peptides from one terminus interact with peptides from the other terminus on the same molecule. In this way, the irregularly shaped hairpins are frustrated from intermolecular stacking into ordered 1D assembled structures. To probe this hypothesis, we prepared π-conjugated peptide solutions over a range of pH from 1 to 7 (10 mM citrate buffer). We assessed the assembled state of these materials using UV−vis absorbance and fluorescence emission, thereby enabling determination of the critical, minimum pH required for the assembly of OT*X* peptides. Interestingly, the critical pH was found to depend on the length of the π-conjugated core. In particular, the critical pH increased from pH 4 for OT4 and OT5 to pH 5 for OT6, which was attributed to solvent-quality effects such that peptides with longer π-conjugated cores are more hydrophobic, which tends to promote assembly. However, for all cases, the critical pH remains near the pK_a for aspartic acid (3.9), which is consistent with the notion that aspartic acid protonation is a critical driving force for assembly. In addition, the relative intensities of the two fluorescence emission peaks for OT5 and OT6 are dependent on pH with the blue-shifted peak becoming more dominant at lower pH. Overall, these data suggest that the assembled morphologies may be sensitive to environmental conditions upon assembly.

We further sought to characterize the dependence of assembled structures on pH. Here, OT4 (0.05 mg/mL in aqueous solution) was assembled over a range of pH values (pH 2, 3, and 4) using diluted HCl and drop-cast onto Si substrates for SEM characterization. Our results show that OT4 assembled at pH 2 and 3 exhibits similar 1D fiber structures previously observed for direct addition of acid (to pH ≈ 1). However, OT4 assembled at pH 4 shows a markedly different morphology, exhibiting large aggregates (several millimeters in diameter) of the assembled peptide (Figure 2). The assembled structure at pH 4 is disordered and highly

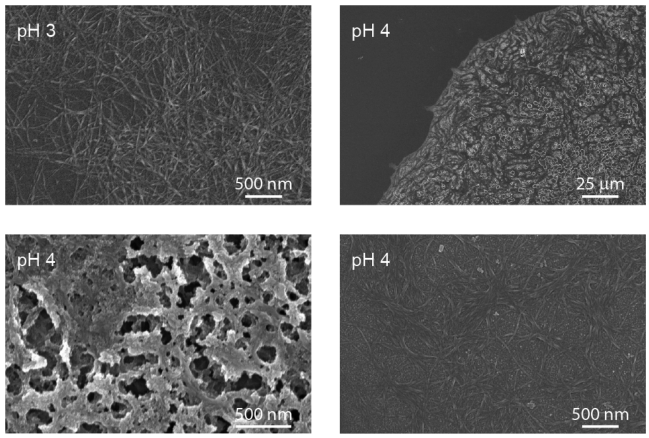

Figure 2. SEM images of DADDG-OT4 as a function of pH. Bottom panels show the images of assembled OT4 in the bulk or interior of the material (left) and near the periphery of the assembled material (right) for large aggregates observed at pH 4.

https://dx.doi.org/10.1021/acsami.0c02095
ACS Appl. Mater. Interfaces 2020, 12, 20722−20732

heterogeneous with some regions showing disordered aggregates and other areas showing some evidence of fibrillation. Interestingly, although some fibers can be observed near the periphery of the aggregates, these fibers are less dense compared to those observed for OT4 at lower pH. We hypothesized that the heterogeneous structures emerged because of the assembly pH near the pKa of aspartic acid residues, which leads to only partial deprotonation of peptides, allowing for aggregation but not ordered assembly.

In order to probe the molecular conformations of π-conjugated peptides under assembly conditions, MD simulations were performed for protonated OT3, OT4, OT5, and OT6 both for single isolated molecules and for solutions of peptide at 10 mM OT*X* (Figure 3). Results from MD

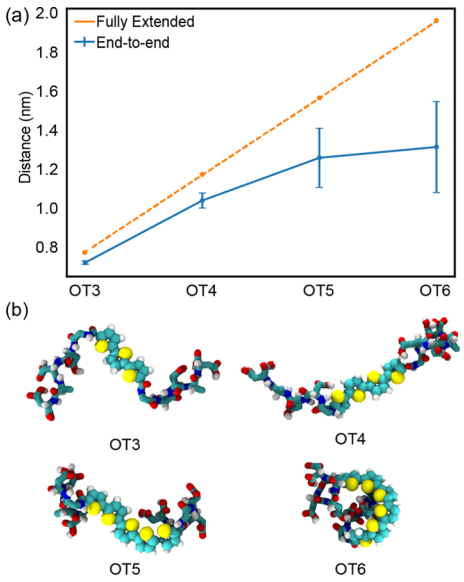

Figure 3. MD simulations of isolated π-conjugated peptides for OT3, OT4, OT5, and OT6. (a) Average end-to-end distance increases sublinearly with the π-conjugated core length. The average end-to-end distance is defined as the center-of-mass separation of the terminal aromatic rings. Error bars correspond to standard errors in the mean end-to-end distance computed by block averaging the 30 ns production run over five contiguous time blocks. (b) Representative snapshots of isolated OT3, OT4, OT5, and OT6 molecules showing relatively linear and extended configurations for OT3, OT4, and OT5 compared to collapsed, folded configurations for OT6.

simulations show that OT*X* molecules exhibit increasingly collapsed single molecule conformations and increased promiscuity in intermolecular interactions upon increasing the length of the π-conjugated core.

Figure 3a shows the average end-to-end distance of isolated OT*X* molecules ($X = 3-6$) from MD simulations. The end-to-end distance increases monotonically with the degree of polymerization of the OT*X* core over this range, but a comparison with the fully extended end-to-end distance shows that molecules with longer π-conjugated cores are significantly more collapsed compared to their fully extended length. This trend can be attributed to the increased flexibility of the longer chains, which permits collapse of the peptide chains into a curved pocket formed by the OT*X* core (Figure 3b). The formation of the curved pocket is most pronounced for OT6 and is mediated by the adoption of cis-configurations of the oligothiophene groups (Figure S12). The intramolecular energetic penalty of these torsional configurations is seemingly compensated by favorable interactions between the core and flanking peptide sequences driven by sequestration of the hydrophobic side chains and formation of intramolecular hydrogen bonds. The elevated preference for curved, collapsed configurations for single oligopeptide chains in their protonated states is expected to further disfavor the formation of assembled 1D ordered structures composed of well-aligned π-stacked oligopeptide chains.

We also explored whether the rigidity of the molecules changed with molecular size. To this end, we computed the Kuhn length b, which is the characteristic length scale over which orientational correlations decay, using the relation $b = \langle R^2 \rangle / L$, where $\langle R^2 \rangle$ is the mean-squared end-to-end distance averaged over the simulation trajectory and L is the fully extended chain length.[49] Standard errors in b are estimated by block averaging over five 6 ns contiguous blocks of the 30 ns trajectory. The Kuhn length for OT3 is $b = 0.700 \pm 0.007$ nm, whereas those for OT4, OT5, and OT6 are indistinguishable within error bars at $b = 0.90 \pm 0.04$, 1.0 ± 0.01, and 0.9 ± 0.2 nm, respectively. For all but the shortest molecule considered, there is no significant trend in the molecular rigidity with chain length and the observed molecular collapse is due primarily to the increasing length of the molecule.

We conducted additional multimolecule molecular simulations to examine the promiscuity of intermolecular contacts between oligopeptides as a function of OT*X* core length. Figure 4 shows the average number of intermolecular contacts per molecule for oligopeptides within a spontaneously self-assembled aggregate consisting of 60 chains formed over the course of a 100 ns molecular simulation. An intermolecular contact is defined using the previously employed "optical distance" measure that judges the cores of two molecules to be in contact if the center-of-mass distance between any pair of

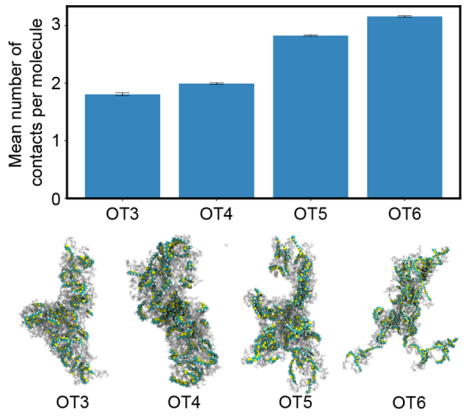

Figure 4. MD simulations of solutions of π-conjugated peptides (OT*X* at 10 mM concentration). Mean number of optical contact neighbors per OT*X* molecule calculated from MD simulations. Averages were calculated over the terminal 60 ns of the production run, and error bars correspond to standard errors in the mean number of contacts per molecule and were computed by block averaging over the final 60 ns of the production run over five contiguous time blocks. OT3 and OT4 possess on average approximately two neighbors, whereas OT5 and OT6 possess approximately three neighbors, leading to increased branching in assembled aggregates for longer core lengths. Characteristic snapshots of each OT*X* system are shown below the plot, where OT*X* cores are represented as van der Waals spheres with carbon rendered blue and sulfur yellow, peptides are faded to translucent gray, and water is removed for clarity.

https://dx.doi.org/10.1021/acsami.0c02095
ACS Appl. Mater. Interfaces 2020, 12, 20722−20732

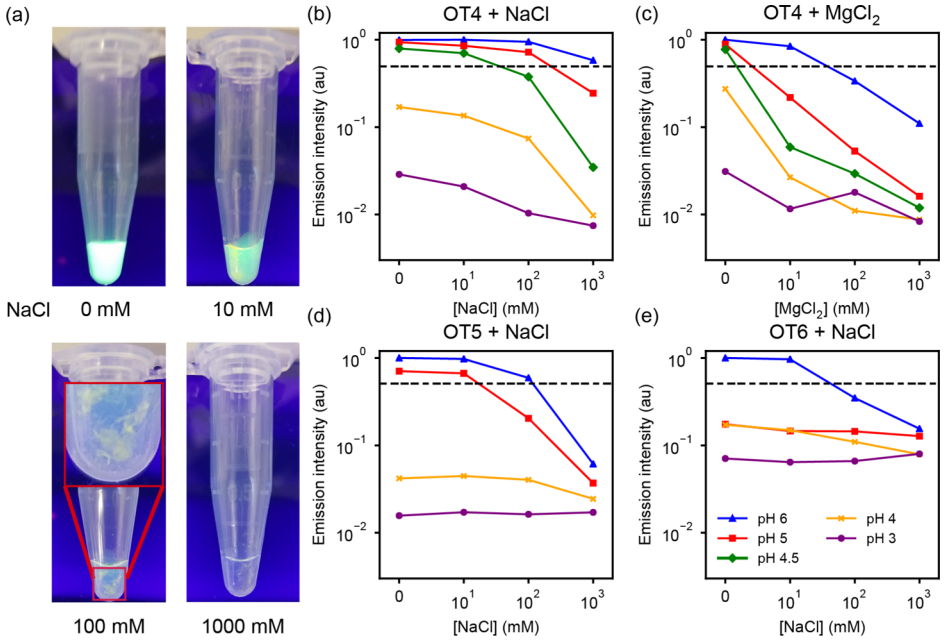

Figure 5. Salt-triggered assembly of DADDG-OT*X* peptides. (a) Photographs of OT4 samples in aqueous solutions (10 mM citrate, pH 4.5) across a range of salt concentrations. (b–e) Fluorescence emission intensity as a function of salt concentration for OT*X* molecules at different solution pH values. Dashed horizontal lines represent 50% fluorescence emission intensity relative to the intensity at the peak emission wavelength of samples at pH 6 with no added salt.

thiophene groups within a cutoff distance of r_{cut} = 0.7 nm.[50,51] OT3 and OT4 molecules possess on average approximately two neighbor contacts, whereas OT5 and OT6 have approximately three neighbors. The increase in the average number of neighbor contacts with molecular size is not surprising given the possibility of more points of intermolecular contact, but these results indicate that π-conjugated peptides with longer cores should tend to be less receptive to assemble into approximately linear 1D structures with exactly two neighbors and high degrees in-registry alignment between the OT*X* cores. These trends are illustrated by the characteristic molecular simulation snapshots in Figure 4.

Taken together, the simulation results highlight the increasing difficulty to induce ordered assembly upon increasing the core length for DADDG-OT*X* peptides: larger OT*X* cores promote intramolecular folding and more promiscuous intermolecular interactions. We note that all simulations performed in this work were conducted for molecules in the fully protonated (i.e., low pH) state. This model corresponds to a hypothetical scenario in which initially dispersed deprotonated (i.e., charged) molecules under high pH are protonated (i.e., made charge neutral) under an instantaneous acid trigger. The conformational distributions of these molecules under basic conditions are expected to differ significantly from those under acidic conditions because of the formal (−4) molecular charge per peptide arm because of the three Asp side chains and C-terminus. We conjecture that these charges may help to prevent molecular collapse and promiscuous aggregation under deprotonated conditions, which suggests a route to the formation of more ordered pseudo-1D assemblies under a protocol in which the pH is slowly lowered from basic to acidic.[48]

Salt-Triggered Assembly of OT*X* Peptides. We further explored additional methods to trigger peptide assembly, moving beyond acid-triggered assembly. We conjectured that electrostatic screening of aspartic acid residues would facilitate intermolecular interactions between peptides, so we pursued salt-triggered assembly by tuning ionic strength. We began by adding a monovalent salt (NaCl, concentrations of 10 mM, 100 mM, and 1.0 M) to an aqueous solution of OT4 (peptide concentration 0.05 mg/mL, pH 6). Similar to the acid-triggered assembly approach, we again used fluorescence emission spectra to characterize the assembly process. Initially, the addition of NaCl was observed to have little effect on the spectral properties of assembled peptides using nonbuffered aqueous solutions, even at a relatively high concentration of 1.0 M NaCl (Figure 5b, blue trace). We reasoned that a combination of mild, acidic pH condition and salt would be more amenable to induce assembly.

Salt-triggered OT4 assembly was then pursued using pH-buffered solutions. Here, we prepared a series of OT4 peptide samples in pH-buffered solutions (10 mM citrate, pH 4.5) across a range of salt concentrations. Evidence of assembly was observed at 1.0 and 0.1 M NaCl but not at lower salt concentration of 10 mM NaCl. In particular, OT4 assembly at 1.0 M NaCl was identified by a significant quenching of fluorescence emission, as well as a red-shifted fluorescence emission peak, consistent with prior experiments on acid-triggered assembly (Table S1). In addition, observation of samples under UV illumination revealed the emergence of a second phase in the high salt (1.0 M, 0.1 M NaCl) samples, exhibiting a visibly distinct yellow-orange coloration (Figure 5a). To further probe the impact of salt concentration on assembly, this procedure was repeated with a divalent salt ($MgCl_2$). Interestingly, the fluorescence emission quenching effect was more pronounced for divalent salt relative to monovalent salt, with appreciable quenching occurring at 10 mM divalent salt (total ionic strength of 30 mM) compared to 100 mM for monovalent salt (Figures 5c, green trace, and S13). These results are consistent with previous studies on peptide aggregation and can be explained by the ability of divalent salts to coordinate acidic residues on neighboring

https://dx.doi.org/10.1021/acsami.0c02095
ACS Appl. Mater. Interfaces 2020, 12, 20722−20732

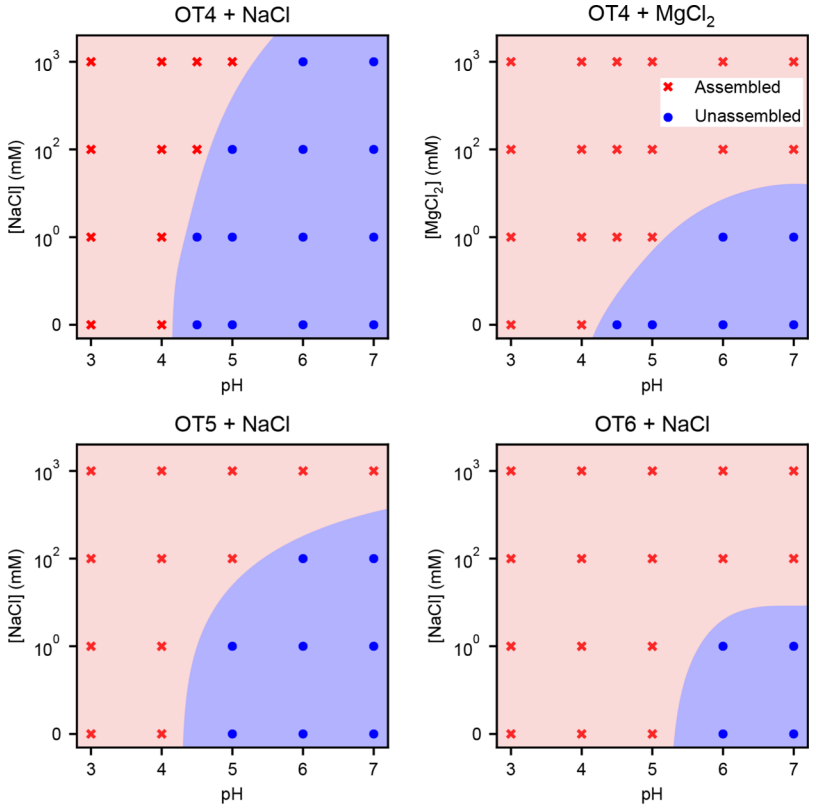

Figure 6. Salt concentration−pH phase diagrams for OT*X* peptide series showing assembled (red) and unassembled (blue) regions. Phase diagrams for OT4 were constructed using monovalent NaCl and divalent $MgCl_2$. Phase diagrams for OT5 and OT6 were constructed using NaCl.

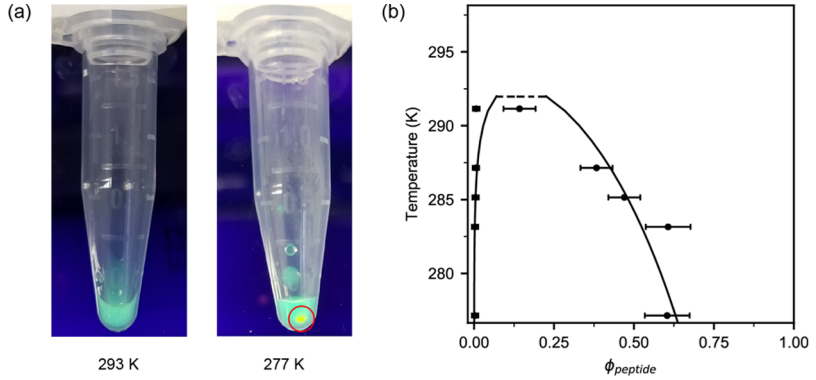

Figure 7. Temperature−concentration phase diagrams for OT4. (a) Representative images of OT4 samples showing a single phase at room temperature (left) and phase separation upon cooling (right). (b) Temperature−concentration phase diagram. The solid line was determined from fitting to the Flory−Huggins free energy equation. The dashed line represents a best-guess estimate of the phase boundary in the limiting region near the UCST.

molecules.[52] Taken together, these results demonstrate that electrostatics can be used to tune the assembly properties of π-conjugated peptides.

Phase Diagrams in pH−Salt Parameter Space. We further sought to determine phase diagrams of peptide assembly in pH−ionic strength parameter space. For these experiments, we prepared solutions of OT*X* peptides (0.05 mg/mL concentration) in pH-buffered aqueous solutions (10 mM citrate buffer) of varying pH and ionic strength. Briefly, addition of salt induced rapid assembly. After incubation for several minutes, peptide solutions were centrifuged to resolve separated phases, followed by determination of absorbance and fluorescence emission spectra of the aqueous phase. As before, fluorescence emission of the aqueous phase was used to track the assembly process, and the fluorescence emission properties were classified into two distinct populations depending on the emission intensity. Briefly, samples with fluorescence emission intensity <50% of the intensity of the neutral pH, no salt sample were considered to be assembled. From these data, we observe that OT5 and OT6 show similar salt-induced quenching behavior compared to OT4 (Figure 5b−e and Tables S1−S4). To validate the emission intensity-based criterion for assembly, samples were centrifuged to resolve separate phases and directly imaged under UV illumination, thereby enabling direct observation of distinct peptide phases. For OT4, we observed a strong correlation between fluorescence quenching and the emergence of a second separated peptide phase (Figures 5a and S13). For OT5 and

https://dx.doi.org/10.1021/acsami.0c02095
ACS Appl. Mater. Interfaces 2020, 12, 20722−20732

OT6, a second phase was not consistently observed by visual inspection on the macroscopic scale (Figures S14 and S15), so the fluorescence emission criterion was used to assess assembly.

Using this approach, phase diagrams were constructed for OT4, OT5, and OT6 in pH−ionic strength parameter space (Figure 6). Broadly speaking, these results show a complex relationship between ionic strength and pH in determining the assembly properties of π-conjugated peptides. In general, lower pH and higher ionic strength lead to peptide assembly. However, the size of the assembled region in the phase diagram generally grows as the length of the π-conjugated core increases. The critical pH at the phase boundary generally follows the trend $pH_{OT4,crit} < pH_{OT5,crit} < pH_{OT6,crit}$, whereas the critical salt concentration at the phase boundary follows the trend $[salt]_{OT4,crit} > [salt]_{OT5,crit} > [salt]_{OT6,crit}$. Furthermore, the phase diagram for OT4 constructed using divalent salt shows a significantly smaller one-phase (unassembled) region such that assembly proceeds under relatively milder conditions at higher pH and lower salt concentrations (Figures 5c and 6). Taken together, these results suggest that peptides with longer π-conjugated cores are more amenable to assembly than those with shorter cores, which is consistent with the role of hydrophobicity in driving the assembly of these materials. Moreover, divalent salts appear to offer a powerful trigger for assembly even under relatively moderate pH conditions.

Phase Diagrams in Temperature−Concentration Space. We further sought to use temperature as an additional trigger of assembly. Here, we experimentally determined phase diagrams for peptide assembly in temperature−peptide concentration phase space (Figure 7). To begin, we prepared aqueous solutions of OT4 (0.05 mg/mL peptide, neutral pH, no added salt) and decreased temperature to 4 °C (277 K). However, these conditions did not lead to peptide assembly, as lower temperatures were not sufficient to overcome the electrostatic repulsion of amino acid residues under these conditions. We next prepared OT4 samples under conditions that were closer to the phase boundary using a pH-buffered solution (0.05 mg/mL peptide, 10 mM citrate, pH 4.5). After equilibrating samples for several days at 4 °C (277 K), the emergence of a second, peptide-rich phase was readily apparent. Moreover, phase separation was not observed in control experiments where peptide solutions were equilibrated at room temperature (20 °C, 293 K) (Figure 7a). Phase diagrams for peptide assembly in temperature−concentration phase space were determined using an analogous method previously reported for determining phase diagrams for self-assembling multivalent DNA nanostars.[53,54] Briefly, peptide solutions (0.05 mg/mL peptide, 10 mM citrate, pH 4.5) were prepared and equilibrated at various temperatures for 5 days. Following equilibration, samples were centrifuged to visually resolve separated phases, followed by spectral analysis of the aqueous supernatant phase using UV−vis absorbance and fluorescence emission. The concentration of peptide in the aqueous phase was determined from absorbance measurements, and the concentration of peptide in the peptide-rich phase was determined by mass balance using the initial concentration of peptide and solution volumes (see the Experimental Methods section). In order to convert mass fraction to volume fraction, the volume fraction of peptide in the peptide-rich phase at low temperature was taken to be $\phi_{peptide} = 0.6$, which is consistent with volume fractions determined for peptide gels based on prior literature.[55]

Using this approach, the phase boundary for peptide assembly was determined in temperature−concentration space (Figure 7b). Our results show that π-conjugated peptides exhibit an asymmetric phase diagram with a coexistence curve showing an upper critical solution temperature (UCST) of approximately 18 °C (291 K) at pH 4.5. In order to quantify peptide assembly, phase diagrams were fit to a binodal coexistence curve obtained from the free energy of mixing using the common tangent method following the Flory−Huggins theory for polymer solutions.[49] In this way, we determined the thermodynamic interaction parameter χ for OT4 peptides in an aqueous environment. This analysis yielded three parameters, including the effective degree of polymerization $N = 40$ and the temperature-dependent parameters for $\chi = A + B/T$, where A and B were found to be −4.46 and 1500 K, respectively. Details of this calculation are provided in the Supporting Information.

CONCLUSIONS

In this work, we use optical and structural characterization to probe the multidimensional phase space of π-conjugated peptide assembly. By varying pH, ionic strength, and temperature, the assembly of OT*X* was established for peptides with four, five, and six thiophene units in the core. Our results show that the final assembled morphologies critically depend on the length of the oligothiophene core. For the OT4 molecules, electron microscopy images of assembled peptides reveal a dense fiber structure accompanied by spectral characteristics indicative of H-aggregates and a macroscopically phase-separated fiber network. However, OT5 and OT6 peptides with the longer thiophene cores show disordered aggregate structures accompanied by emission spectra with both a blue-shifted and a red-shifted local maximum, together with no visible evidence of macroscopic phase separation. MD simulations suggest that the disordered assembly results from a combination of intramolecular folding as well as promiscuous slip-stacked packing for the larger OT*X* cores that inhibited long-range order.

For OT4, OT5, and OT6 peptides, phase diagrams were constructed in pH−ionic strength phase space. Overall, these results demonstrate the complex dynamic interplay between the ionic strength and acidity/basicity in determining the phase peptide solutions. Furthermore, changes to core length caused significant changes in the phase behavior, such that the one-phase envelope decreased in size upon increasing the thiophene core length because of increasingly dominant hydrophobic interactions. Finally, a phase diagram for OT4 was constructed in temperature−concentration space, demonstrating that temperature can be used as an additional trigger of assembly. Moreover, these experiments enabled determination of key thermodynamic parameters such as the Flory−Huggins χ parameter and the critical conditions for assembly.

The results presented in this work provide critical insights for both the materials design and processing aspects of organic electronics. The dependence of assembled morphologies on the molecular core structure demonstrates that the design of biohybrid electronic materials requires a careful balance between desirable electronic properties and materials assembly behavior. As one example, although increasing molecular size may yield improved electronic properties because of smaller band gaps, there is an unexpected trade-off resulting from decreasing order in assembled morphologies upon increasing the molecular size. On the other hand, the pH-dependent

https://dx.doi.org/10.1021/acsami.0c02095
ACS Appl. Mater. Interfaces 2020, 12, 20722−20732

assembly of OT4 shows the potential for tuning environmental conditions and external parameters for controlling assembled morphologies.

The phase diagrams determined in this work provide significant insights into the assembly properties of π-conjugated oligopeptide materials. The phase boundaries could provide a useful framework for determining critical conditions for solution processing of organogel-based electronics. Furthermore, the demonstration of significant core sequence effects on assembly helps to further elucidate key design principles for sequence-defined organic electronics. Broadly speaking, the phase diagrams presented in this work provide a clearly defined window of environmental conditions over which these materials can be processed to yield ordered, organic semiconductor thin films for the development of organic transistors. In addition, our work clearly explores multiple external triggers for controlling assembly, thereby providing several processing routes for these materials. Furthermore, our results show that the ionic strength and temperature can be used to control the assembly of these materials under biologically relevant conditions, which avoids the use of highly acidic conditions for assembly that may not be suitable for most biological systems. Taken together, our results show that a variety of factors—environmental and structural—can be used to control the assembly of supramolecular organic electronics.

■ ASSOCIATED CONTENT

Supporting Information

The Supporting Information is available free of charge at https://pubs.acs.org/doi/10.1021/acsami.0c02095.

Detailed methods for fitting phase diagram data with Flory−Huggins theory; characterization details for conjugated peptides including ^{1}H NMR, ESI-MS, and HPLC; summary of spectral data used in the development of phase diagrams; photographs of OT*X* samples showing macroscopic phase separation and quenching; DLS results for OT6 showing aggregation and particle size; TEM micrographs of OT*X* peptides; and additional simulation results showing tacticity of OT*X* molecules (PDF)

■ AUTHOR INFORMATION

Corresponding Author

Charles M. Schroeder − *Department of Chemical and Biomolecular Engineering and Beckman Institute for Advanced Science and Technology, University of Illinois at Urbana-Champaign, Urbana, Illinois 61801, United States;* orcid.org/0000-0001-6023-2274; Email: cms@illinois.edu

Authors

Edward R. Jira − *Department of Chemical and Biomolecular Engineering and Beckman Institute for Advanced Science and Technology, University of Illinois at Urbana-Champaign, Urbana, Illinois 61801, United States*

Kirill Shmilovich − *Pritzker School of Molecular Engineering, University of Chicago, Chicago, Illinois 60637, United States*

Tejaswini S. Kale − *Department of Chemistry, Johns Hopkins University, Baltimore, Maryland 21218, United States;* orcid.org/0000-0001-7246-745X

Andrew Ferguson − *Pritzker School of Molecular Engineering, University of Chicago, Chicago, Illinois 60637, United States;* orcid.org/0000-0002-8829-9726

John D. Tovar − *Department of Chemistry, Johns Hopkins University, Baltimore, Maryland 21218, United States;* orcid.org/0000-0002-9650-2210

Complete contact information is available at: https://pubs.acs.org/10.1021/acsami.0c02095

Notes

The authors declare no competing financial interest.

■ ACKNOWLEDGMENTS

This research was partially supported by the NSF through the University of Illinois at Urbana-Champaign Materials Research Science and Engineering Center (I-MRSEC) DMR-1720633. Structural characterization was carried out in part in the Materials Research Laboratory Central Research Facilities, University of Illinois. This material is based upon the work supported by the National Science Foundation under grant no. DMR-1841807 and a National Science Foundation Graduate Research Fellowship to K.S. under grant no. DGE-1746045. This work was completed in part with resources provided by the University of Chicago Research Computing Center. We gratefully acknowledge computing time on the University of Chicago high-performance GPU-based cyberinfrastructure (grant no. DMR-1828629).

■ REFERENCES

(1) Gelinck, G. H.; Huitema, H. E. A.; van Veenendaal, E.; Cantatore, E.; Schrijnemakers, L.; Van Der Putten, J. B. P. H.; Geuns, T. C. T.; Beenhakkers, M.; Giesbers, J. B.; Huisman, B.-H.; Meijer, E. J.; Benito, E. M.; Touwslager, F. J.; Marsman, A. W.; Van Rens, B. J. E.; de Leeuw, D. M. Flexible Active-Matrix Displays and Shift Registers Based on Solution-Processed Organic Transistors. *Nat. Mater.* **2004**, *3*, 106−110.

(2) Oh, J. Y.; Rondeau-Gagné, S.; Chiu, Y.-C.; Chortos, A.; Lissel, F.; Wang, G.-J. N.; Schroeder, B. C.; Kurosawa, T.; Lopez, J.; Katsumata, T.; Xu, J.; Zhu, C.; Gu, X.; Bae, W.-G.; Kim, Y.; Jin, L.; Chung, J. W.; Tok, J. B.-H.; Bao, Z. Intrinsically Stretchable and Healable Semiconducting Polymer for Organic Transistors. *Nature* **2016**, *539*, 411−415.

(3) Tee, B. C. K. A Skin-Inspired Organic Digital Mechanoreceptor. *Science* **2015**, *350*, 313.

(4) Sirringhaus, H. 25th Anniversary Article: Organic Field-Effect Transistors: The Path Beyond Amorphous Silicon. *Adv. Mater.* **2014**, *26*, 1319−1335.

(5) Bittle, E. G.; Ro, H. W.; Snyder, C. R.; Engmann, S.; Kline, R. J.; Zhang, X.; Jurchescu, O. D.; DeLongchamp, D. M.; Gundlach, D. J. Dependence of Electrical Performance on Structural Organization in Polymer Field Effect Transistors. *J. Polym. Sci., Part B: Polym. Phys.* **2017**, *55*, 1063−1074.

(6) Rivnay, J.; Jimison, L. H.; Northrup, J. E.; Toney, M. F.; Noriega, R.; Lu, S.; Marks, T. J.; Facchetti, A.; Salleo, A. Large Modulation of Carrier Transport by Grain-Boundary Molecular Packing and Microstructure in Organic Thin Films. *Nat. Mater.* **2009**, *8*, 952−958.

(7) Moonen, P. F.; Yakimets, I.; Huskens, J. Fabrication of Transistors on Flexible Substrates: From Mass-Printing to High-Resolution Alternative Lithography Strategies. *Adv. Mater.* **2012**, *24*, 5526−5541.

(8) Na, J. Y.; Kang, B.; Sin, D. H.; Cho, K.; Park, Y. D. Understanding Solidification of Polythiophene Thin Films During Spin-Coating: Effects of Spin-Coating Time and Processing Additives. *Sci. Rep.* **2015**, *5*, 13288.

(9) Anthony, J. E. Functionalized Acenes and Heteroacenes for Organic Electronics. *Chem. Rev.* **2006**, *106*, 5028−5048.

(10) Guan, Y.-S.; Qin, Y.; Sun, Y.; Wang, C.; Xu, W.; Zhu, D. Single-Bundle Nanofiber Based OFETs Fabricated from a Cyclic Conjugated Organogelator with High Field-Effect Mobility and High Photoresponsivity. *Chem. Commun.* **2015**, *51*, 12182−12184.
(11) Hong, J.-P.; Um, M.-C.; Nam, S.-R.; Hong, J.-I.; Lee, S. Organic Single-Nanofiber Transistors from Organogels. *Chem. Commun.* **2009**, 310−312.
(12) Ghosh, S.; Praveen, V. K.; Ajayaghosh, A. The Chemistry and Applications of π-Gels. *Annu. Rev. Mater. Res.* **2016**, *46*, 235−262.
(13) Giansante, C.; Raffy, G.; Schäfer, C.; Rahma, H.; Kao, M.-T.; Olive, A. G. L.; Del Guerzo, A. White-Light-Emitting Self-Assembled Nanofibers and Their Evidence by Microspectroscopy of Individual Objects. *J. Am. Chem. Soc.* **2011**, *133*, 316−325.
(14) Stupp, S. I.; Palmer, L. C. Supramolecular Cemistry and Self-Assembly in Organic Materials Design. *Chem. Mater.* **2014**, *26*, 507−518.
(15) Hughes, M.; Xu, H.; Frederix, P. W. J. M.; Smith, A. M.; Hunt, N. T.; Tuttle, T.; Kinloch, I. A.; Ulijn, R. V. Biocatalytic Self-Assembly of 2D Peptide-Based Nanostructures. *Soft Matter* **2011**, *7*, 10032−10038.
(16) Castelletto, V.; Hamley, I. W.; Perez, J.; Abezgauz, L.; Danino, D. Fibrillar Superstructure from Extended Nanotapes Formed by a Collagen-Stimulating Peptide. *Chem. Commun.* **2010**, *46*, 9185−9187.
(17) Kim, W.; Thévenot, J.; Ibarboure, E.; Lecommandoux, S.; Chaikof, E. L. Self-Assembly of Thermally Responsive Amphiphilic Diblock Copolypeptides into Spherical Micellar Nanoparticles. *Angew. Chem., Int. Ed.* **2010**, *49*, 4257−4260.
(18) Hartgerink, J. D.; Beniash, E.; Stupp, S. I. Self-Assembly and Mineralization of Peptide-Amphiphile Nanofibers. *Science* **2001**, *294*, 1684−1688.
(19) Schillinger, E.-K.; Mena-Osteritz, E.; Hentschel, J.; Börner, H. G.; Bäuerle, P. Oligothiophene Versus β-Sheet Peptide: Synthesis and Self-Assembly of an Organic Semiconductor-Peptide Hybrid. *Adv. Mater.* **2009**, *21*, 1562−1567.
(20) Choi, I.; Park, I.-S.; Ryu, J.-H.; Lee, M. Control of Peptide Assembly Through Directional Interactions. *Chem. Commun.* **2012**, *48*, 8481−8483.
(21) Tang, C.; Ulijn, R. V.; Saiani, A. Effect of Glycine Substitution on Fmoc-Diphenylalanine Self-Assembly and Gelation Properties. *Langmuir* **2011**, *27*, 14438−14449.
(22) Lehrman, J. A.; Cui, H.; Tsai, W.-W.; Moyer, T. J.; Stupp, S. I. Supramolecular Control of Self-Assembling Terthiophene-Peptide Conjugates Through the Amino Acid Side Chain. *Chem. Commun.* **2012**, *48*, 9711−9713.
(23) Baumann, M. K.; Textor, M.; Reimhult, E. Understanding Self-Assembled Amphiphilic Peptide Supramolecular Structures From Primary Structure Helix Propensity. *Langmuir* **2008**, *24*, 7645−7647.
(24) Draper, E. R.; Morris, K. L.; Little, M. A.; Raeburn, J.; Colquhoun, C.; Cross, E. R.; McDonald, T. O.; Serpell, L. C.; Adams, D. J. Hydrogels Formed from Fmoc Amino Acids. *CrystEngComm* **2015**, *17*, 8047−8057.
(25) Ardoña, H. A. M.; Tovar, J. D. Peptide π-Electron Conjugates: Organic Electronics for Biology? *Bioconjugate Chem.* **2015**, *26*, 2290−2302.
(26) Li, B.; Li, S.; Zhou, Y.; Ardoña, H. A. M.; Valverde, L. R.; Wilson, W. L.; Tovar, J. D.; Schroeder, C. M. Nonequilibrium Self-Assembly of π-Conjugated Oligopeptides in Solution. *ACS Appl. Mater. Interfaces* **2017**, *9*, 3977−3984.
(27) Ardoña, H. A. M.; Draper, E. R.; Citossi, F.; Wallace, M.; Serpell, L. C.; Adams, D. J.; Tovar, J. D. Kinetically Controlled Coassembly of Multichromophoric Peptide Hydrogelators and the Impacts on Energy Transport. *J. Am. Chem. Soc.* **2017**, *139*, 8685−8692.
(28) Wall, B. D.; Zacca, A. E.; Sanders, A. M.; Wilson, W. L.; Ferguson, A. L.; Tovar, J. D. Supramolecular Polymorphism: Tunable Electronic Interactions Within π-Conjugated Peptide Nanostructures Dictated by Primary Amino Acid Sequence. *Langmuir* **2014**, *30*, 5946−5956.
(29) Zhou, Y.; Li, B.; Li, S.; Ardoña, H. A. M.; Wilson, W. L.; Tovar, J. D.; Schroeder, C. M. Concentration-Driven Assembly and Sol-Gel Transition of π-Conjugated Oligopeptides. *ACS Cent. Sci.* **2017**, *3*, 986−994.
(30) Besar, K.; Ardoña, H. A. M.; Tovar, J. D.; Katz, H. E. Demonstration of Hole Transport and Voltage Equilibration in Self-Assembled π-Conjugated Peptide Nanostructures Using Field-Effect Transistor Architectures. *ACS Nano* **2015**, *9*, 12401−12409.
(31) Zhao, H.; Zhu, B.; Sekine, J.; Luo, S.-C.; Yu, H.-h. Oligoethylene-Glycol-Functionalized Polyoxythiophenes for Cell Engineering: Syntheses, Characterizations, and Cell Compatibilities. *ACS Appl. Mater. Interfaces* **2012**, *4*, 680−686.
(32) Wigenius, J.; Persson, G.; Widengren, J.; Inganäs, O. Interactions Between a Luminescent Conjugated Oligoelectrolyte and Insulin During Early Phases of Amyloid Formation. *Macromol. Biosci.* **2011**, *11*, 1120−1127.
(33) Vadehra, G. S.; Wall, B. D.; Diegelmann, S. R.; Tovar, J. D. On-Resin Dimerization Incorporates a Diverse Array of π-Conjugated Functionality Within Aqueous Self-Assembling Peptide Backbones. *Chem. Commun.* **2010**, *46*, 3947−3949.
(34) Abraham, M. J.; Murtola, T.; Schulz, R.; Páll, S.; Smith, J. C.; Hess, B.; Lindahl, E. Gromacs: High Performance Molecular Simulations Through Multi-Level Parallelism From Laptops to Supercomputers. *SoftwareX* **2015**, *1−2*, 19−25.
(35) Koziara, K. B.; Stroet, M.; Malde, A. K.; Mark, A. E. Testing and Validation of the Automated Topology Builder (ATB) Version 2.0: Prediction of Hydration Free Enthalpies. *J. Comput.-Aided Mol. Des.* **2014**, *28*, 221−233.
(36) Schmid, N.; Eichenberger, A. P.; Choutko, A.; Riniker, S.; Winger, M.; Mark, A. E.; Van Gunsteren, W. F. Definition and Testing of the GROMOS Force-Field Versions 54A7 and 54B7. *Eur. Biophys. J.* **2011**, *40*, 843−856.
(37) Berendsen, H. J. C.; Postma, J. P. M.; van Gunsteren, W. F.; Hermans, J. In *Intermolecular Forces: Proceedings of the Fourteenth Jerusalem Symposium on Quantum Chemistry and Biochemistry Held in Jerusalem, Israel, April 13−16, 1981*; Pullman, B., Ed.; Springer Netherlands: Dordrecht, 1981; pp 331−342.
(38) Bussi, G.; Donadio, D.; Parrinello, M. Canonical Sampling Through Velocity Rescaling. *J. Chem. Phys.* **2007**, *126*, 014101.
(39) Parrinello, M.; Rahman, A. Polymorphic Transitions in Single Crystals: A New Molecular Dynamics Method. *J. Appl. Phys.* **1981**, *52*, 7182−7190.
(40) Hockney, R. W.; Eastwood, J. *Computer Simulations Using Particles*; Taylor & Francis, Inc., 1988.
(41) Essmann, U.; Perera, L.; Berkowitz, M. L.; Darden, T.; Lee, H.; Pedersen, L. G. A Smooth Particle Mesh Ewald Method. *J. Chem. Phys.* **1995**, *103*, 8577−8593.
(42) Hess, B.; Bekker, H.; Berendsen, H. J. C.; Fraaije, J. G. E. M. LINCS: A Linear Constraint Solver for Molecular Simulations. *J. Comput. Chem.* **1997**, *18*, 1463−1472.
(43) Grebner, D.; Helbig, M.; Rentsch, S. Size-Dependent Properties of Oligothiophenes by Picosecond Time-Resolved Spectroscopy. *J. Phys. Chem.* **1995**, *99*, 16991−16998.
(44) Kale, T. S.; Ardoña, H. A. M.; Ertel, A.; Tovar, J. D. Torsional Impacts on Quaterthiophene Segments Confined Within Peptidic Nanostructures. *Langmuir* **2019**, *35*, 2270.
(45) Marciel, A. B.; Tanyeri, M.; Wall, B. D.; Tovar, J. D.; Schroeder, C. M.; Wilson, W. L. Fluidic-Directed Assembly of Aligned Oligopeptides with π-Conjugated Cores. *Adv. Mater.* **2013**, *25*, 6398−6404.
(46) Wall, B. D.; Tovar, J. D. Synthesis and Characterization of π-Conjugated Peptide-Based Supramolecular Materials. *Pure Appl. Chem.* **2012**, *84*, 1039−1045.
(47) Spano, F. C. The Spectral Signatures of Frenkel Polarons in H- and J-Aggregates. *Acc. Chem. Res.* **2010**, *43*, 429−439.
(48) Sanders, A. M.; Dawidczyk, T. J.; Katz, H. E.; Tovar, J. D. Peptide-Based Supramolecular Semiconductor Nanomaterials via Pd-Catalyzed Solid-Phase "Dimerizations". *ACS Macro Lett.* **2012**, *1*, 1326−1329.

https://dx.doi.org/10.1021/acsami.0c02095
ACS Appl. Mater. Interfaces 2020, 12, 20722−20732

(49) Rubinstein, M.; Colby, R. H. *Polymer Physics*; Oxford University Press: Oxford, 2003.
(50) Mansbach, R. A.; Ferguson, A. L. Control of the Hierarchical Assembly of π-Conjugated Optoelectronic Peptides by pH and Flow. *Org. Biomol. Chem.* **2017**, *15*, 5484−5502.
(51) Mansbach, R. A.; Ferguson, A. L. Coarse-Grained Molecular Simulation of the Hierarchical Self-Assembly of π-Conjugated Optoelectronic Peptides. *J. Phys. Chem. B* **2017**, *121*, 1684−1706.
(52) Gallaher, J. K.; Aitken, E. J.; Keyzers, R. A.; Hodgkiss, J. M. Controlled Aggregation of Peptide-Substituted Perylene-Bisimides. *Chem. Commun.* **2012**, *48*, 7961−7963.
(53) Biffi, S.; Cerbino, R.; Bomboi, F.; Paraboschi, E. M.; Asselta, R.; Sciortino, F.; Bellini, T. Phase Behavior and Critical Activated Dynamics of Limited-Valence DNA Nanostars. *Proc. Natl. Acad. Sci. U.S.A.* **2013**, *110*, 15633−15637.
(54) Biffi, S.; Cerbino, R.; Nava, G.; Bomboi, F.; Sciortino, F.; Bellini, T. Equilibrium Gels of Low-Valence DNA Nanostars: A Colloidal Model for Strong Glass Formers. *Soft Matter* **2015**, *11*, 3132−3138.
(55) Dumetz, A. C.; Chockla, A. M.; Kaler, E. W.; Lenhoff, A. M. Protein Phase Behavior in Aqueous Solutions: Crystallization, Liquid-Liquid Phase Separation, Gels, and Aggregates. *Biophys. J.* **2008**, *94*, 570−583.

https://dx.doi.org/10.1021/acsami.0c02095
ACS Appl. Mater. Interfaces 2020, 12, 20722−20732